Available online at www.sciencedirect.com

SciVerse ScienceDirect

Journal of the European Ceramic Society 32 (2012) 2137–2143

www.elsevier.com/locate/jeurceramsoc

Solidification of Al_2O_3–YAG eutectic composites with off-metastable eutectic composition from undercooled melt produced by melting Al_2O_3–YAP eutectics

Tomoya Nagira *, Hideyuki Yasuda, Takumi Sakimura, Kentarou Yoshida

Department of Adaptive Machine Systems, Osaka University, Suita 565-0871, Japan

Received 16 November 2011; received in revised form 3 February 2012; accepted 6 February 2012
Available online 3 March 2012

Abstract

It has been reported that solidification of the Al_2O_3–YAG equilibrium eutectic structure follows melting of the Al_2O_3–YAP metastable eutectic structure. Since the exothermic heat due to solidification was consumed by the endothermic heat due to melting, a fine and uniform eutectic structure was obtained. However, the composition of the Al_2O_3–YAG eutectic structure is restricted to the metastable eutectic composition. In this paper, Al_2O_3–YAG eutectic compacts with an off-metastable eutectic composition were prepared by the addition of Al_2O_3 particles to Al_2O_3–YAP eutectic particles with diameters less than 20 μm. In compositions ranging from 18.5 mol%Y_2O_3 to 13.5 mol%Y_2O_3, dense Al_2O_3–YAG eutectic compacts were formed without any Al_2O_3 segregation. The flexural strength and the fracture toughness remained almost unchanged with the increase in the Al_2O_3 phase. The addition of Al_2O_3 particles to the Al_2O_3–YAP eutectic particles enabled the matrix phase to change from the YAG phase to the Al_2O_3 phase.

Keywords: Composites; Al_2O_3; Eutectic; Shaping

1. Introduction

The development of unidirectional solidified Al_2O_3–based eutectic ceramic composites such as Al_2O_3–YAG ($Y_3Al_5O_{12}$: yttrium–aluminum–garnet), Al_2O_3–EAG ($Er_3Al_5O_{12}$: erbium–aluminum–garnet), and Al_2O_3–GAP ($GaAlO_3$:gallium –aluminum–perovskite) systems is of considerable importance because these composites have superior mechanical properties at elevated temperatures.[1–5] Waku et al. reported that unidirectional solidified eutectic composites consisting of a single crystal Al_2O_3 and a single crystal YAG had a flexural strength of 360–400 MPa at room temperature to 2073 K.[3–5] In addition to research on its mechanical properties at elevated temperatures, interesting solidification phenomena in the Al_2O_3–Y_2O_3 system have been reported.[6–8] Caslavsky and Viechnickl reported that two eutectic reactions of the Al_2O_3–YAG eutectic reaction at 2099 K and an Al_2O_3–YAP ($YAlO_3$:yttrium–aluminum–perovskite) eutectic reaction at 1975 K existed in the Al_2O_3-rich portion of the Al_2O_3–Y_2O_3 phase diagram as shown in Fig. 1.[8] Solidification of the Al_2O_3–YAP metastable eutectic path occurs at a composition range of 13.5–28.5 mol%Y_2O_3.[8–10] Heating the melt with the metastable eutectic composition above 2273 K causes the Al_2O_3–YAP metastable eutectic structure to be indispensably selected.

Our previous papers[9–17] have showed that an undercooled melt is produced by heating the Al_2O_3–YAP metastable eutectic structure to temperatures between the metastable eutectic temperature and the equilibrium eutectic temperature. Solidification of the Al_2O_3–YAG equilibrium eutectic system follows formation of the undercooled melt. Coupling the solidification of the Al_2O_3–YAG equilibrium eutectic structure and melting of the Al_2O_3–YAP metastable eutectic structure leads to a higher growth velocity of 10^{-3} m/s, resulting in the formation of a fine eutectic structure. Additionally, the 11% volume expansion in the transformation from the Al_2O_3 phase and the YAP phase to the YAG phase reduces the porosity of the castings. This novel solidification process using the undercooled melt formed by the melting of the Al_2O_3–YAP metastable eutectic structure is effective for preparing dense Al_2O_3–YAG eutectic compacts

* Corresponding author. Tel.: +81 6 6879 7476; fax: +81 6 6879 7476.
E-mail address: nagira@ams.eng.osaka-u.ac.jp (T. Nagira).

0955-2219/$ – see front matter © 2012 Elsevier Ltd. All rights reserved.
doi:10.1016/j.jeurceramsoc.2012.02.007

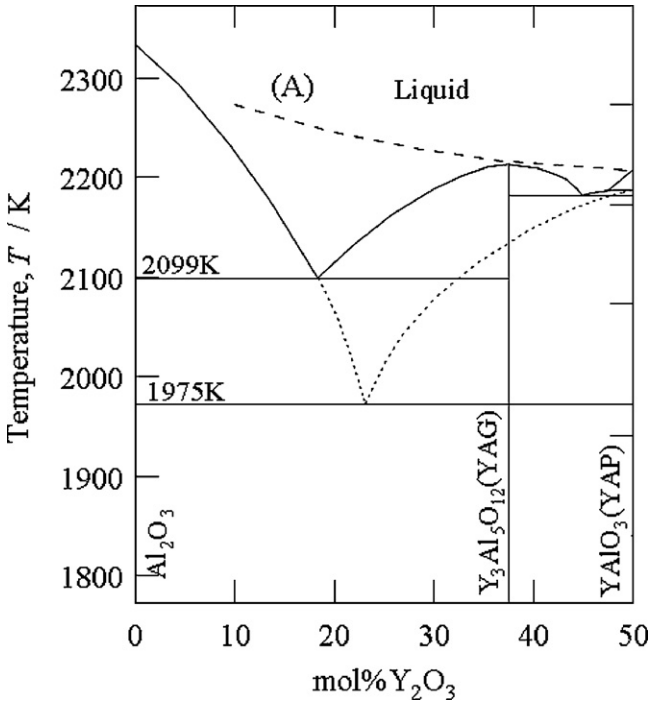

Fig. 1. Phase diagram of Al_2O_3–Y_2O_3 system. The pecked lines indicate the liquidus of the metastable eutectic system. Melts cooled from the temperatures above the dashed line (A) follow the solidification in metastable path.[8]

with a fine microstructure. Unfortunately, the composition of the Al_2O_3–YAG eutectic structure is limited to the metastable eutectic composition because the Al_2O_3–YAP metastable eutectic structure without any primary phases is only obtained at the metastable eutectic composition.

The room-temperature flexural strength of the Al_2O_3–YAG eutectic compact formed by solidification accompanying melting of the Al_2O_3–YAP metastable eutectic structure has been reported.[16] The Al_2O_3–YAG eutectic compact produced using Al_2O_3–YAP eutectic particles with diameters less than 20 μm had a room-temperature flexural strength of 339 MPa. In the metastable eutectic composition, the matrix phase is the YAG phase, whose fracture toughness is lower than that of the Al_2O_3 phase.[18] An increase in the volume fraction of the Al_2O_3 phase can result in an improvement in its mechanical properties.

It has been reported[11] that solidification of the Al_2O_3–YAG–ZrO_2 equilibrium eutectic structure accompanies melting of the Al_2O_3–YAP–ZrO_2 metastable eutectic structure, which is essentially the same solidification phenomenon that occurs in the Al_2O_3–Y_2O_3 system. It should be noted that the partially Y_2O_3-stabilized ZrO_2 (YSZ) phase, which has ionic conductivity, is formed through a eutectic reaction. Accordingly, increasing the volume fraction of the YSZ phase in Al_2O_3–YAG–ZrO_2 equilibrium eutectic composites is expected to lead to development of functionalized Al_2O_3-based eutectic ceramics.

Therefore, it is important to develop a process for preparing Al_2O_3–YAG eutectic composites over a wide range of compositions to expand the application of Al_2O_3–YAG eutectic composites. A few processes for the fabrication of Al_2O_3-based eutectic composites with off-eutectic composition have been reported.[19,20] In this study, a new method in which the solidification process was modified utilizing the undercooled melt produced by melting of the Al_2O_3–YAP metastable eutectic structure is proposed. In this process, Al_2O_3 particles are added to the Al_2O_3–YAP eutectic particles to prepare Al_2O_3–YAG eutectic composites with a hypo-metastable eutectic composition. According to the phase diagram of the Al_2O_3–YAP metastable eutectic system shown in Fig. 1, the added Al_2O_3 particles can be partially melted at temperatures between the metastable eutectic temperature and the equilibrium eutectic temperature. In addition, the Al_2O_3–YAP metastable eutectic specimen is expected to start melting at the Al_2O_3/YAP phase boundaries. Therefore, if the added Al_2O_3 particles are sintered with the Al_2O_3–YAP metastable eutectic particles before the melting temperature is reached, the added Al_2O_3 particles will melt. Al_2O_3 particles with diameter of 1 μm, which is considerably smaller than the diameter of Al_2O_3–YAP eutectic particles (<20 μm), are used to facilitate formation of the Al_2O_3/YAP phase boundaries between the added Al_2O_3 particles and the Al_2O_3–YAP eutectic particles.

This paper presents the fabrication of an Al_2O_3–YAG eutectic compact with an off-metastable eutectic composition by adding Al_2O_3 particles with diameter of 1 μm to Al_2O_3–YAP eutectic particles with diameters of less than 20 μm. The microstructures of Al_2O_3–YAG eutectic compacts with off-metastable eutectic compositions of Al_2O_3–x mol%Y_2O_3 (x = 18.5, 15, 13.5, 10.5, and 8.5) and their flexural strengths and fracture toughness are compared to those of the Al_2O_3–YAG eutectic compact produced by the melting of the Al_2O_3–YAP eutectic particles with diameters of less than 20 μm. The influences of the addition of Al_2O_3 particles to Al_2O_3–YAP eutectic particles on the formation of the Al_2O_3–YAG eutectic compact are also discussed.

2. Experimental procedure

α-Al_2O_3 powder (99.99%) and Y_2O_3 powder (99.99%) were weighed according to the Al_2O_3–23.5 mol%Y_2O_3, which is the Al_2O_3–YAP metastable eutectic composition. Their powders were ball milled with ethanol for 24 h to obtain a homogeneous slurry that was subsequently dried in a vacuum. The mixed powder was melted in a Mo crucible using an induction furnace in an Ar atmosphere. The Al_2O_3–YAP metastable eutectic structure was obtained by heating the melt to temperatures above 2300 K before solidification. The solidified specimens were crushed into particles. Al_2O_3–YAP metastable eutectic particles with diameters less than 20 μm were used in this study. The obtained Al_2O_3–YAP eutectic grains and α-Al_2O_3 particles (99.99%, 1 μm diameter) were ball milled with ethanol for 24 h according to the Al_2O_3–x mol%Y_2O_3 (x = 18.5, 15, 13.5, 10.5, and 8.5). The mixed particles were then inserted into a Mo mold with an outer diameter of 10 mm and an inner diameter of 6 mm. The Mo mold was inserted into a carbon die and α-Al_2O_3 powder was then added to avoid the energization of the Mo die. The carbon die was subsequently heated to 2023 K at a rate of 1.7 K/s under a pressure of 40 MPa. The specimen was kept at 2023 K in vacuum for 60 s. The microstructures of the specimens

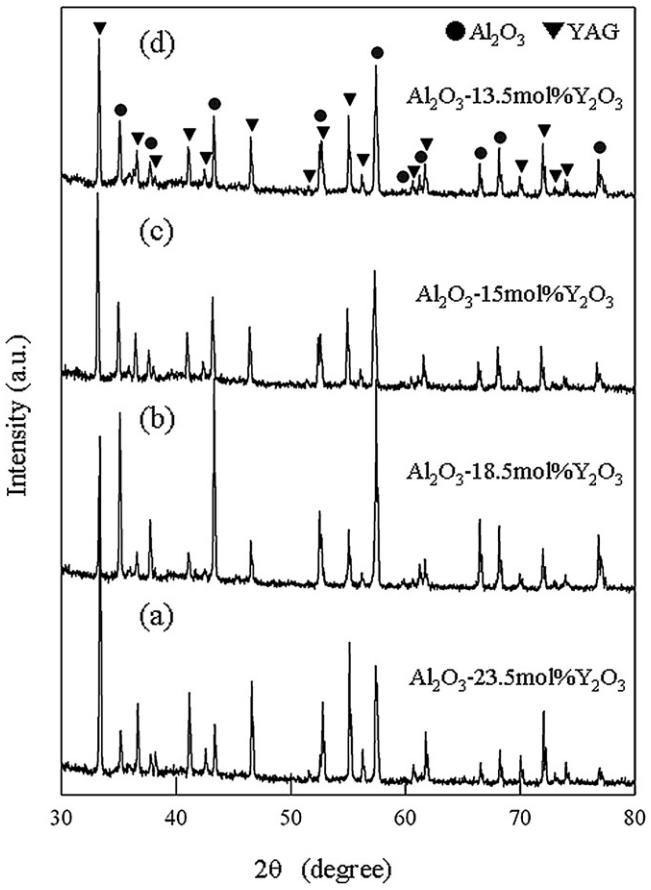

Fig. 2. X-ray diffraction patterns of specimens with compositions of Al_2O_3–x mol%Y_2O_3: x = (a) 23.5 (b) 18.5 (c) 15.0, and (d) 13.5.

were observed using scanning electron microscopy (SEM). The lamellar spacing is numerically estimated from interfacial length per unit area. Details of the evaluation are given in the previous paper.[12] The density of the Al_2O_3–YAG eutectic compacts was measured by Archimedes' principle. The crystal structures were examined by X-ray diffraction (XRD) analysis using Cu Kα radiation. The flexural strength was measured using the three-point bending technique over a span of 10 mm and at a cross-head speed of 0.1 mm/min. A specimen with dimensions of 1 mm × 2 mm × 13 mm was used for the flexural strength test and their surfaces were polished with #400 emery paper in the perpendicular direction to the flexural axis. The hardness (H) and the fracture toughness (K_{IC}) were measured using a Vickers hardness tester under a load of 5 kgf. The values of fracture toughness were calculated using the equation proposed by Anstis et al.[21,22] The Young's modulus was taken from the reference.[23]

3. Results and discussion

3.1. Formation of Al_2O_3–YAG eutectic compact with off-metastable eutectic composition

X-ray diffraction patterns of specimens with compositions of Al_2O_3–x mol%Y_2O_3 (x = 18.5, 15.0, and 13.5) are shown in Fig. 2(b)–(d). For comparison, Fig. 2(a) shows the X-ray diffraction patterns of the Al_2O_3–YAG eutectic compact (Al_2O_3–23.5 mol%Y_2O_3) produced by melting Al_2O_3–YAP metastable eutectic particles with diameters less than 20 μm.[16] The diffraction peaks for all specimens were assigned to an α-Al_2O_3 phase and a YAG phase. For all compositions, Al_2O_3–YAG eutectic compacts were formed by using the mixtures of Al_2O_3–YAP eutectic particles and Al_2O_3 particles.

Fig. 3(a)–(f) shows the microstructures of Al_2O_3–YAG eutectic compacts with various compositions of Al_2O_3–x mol%Y_2O_3 (x = 23.5, 18.5, 15.0, 13.5, 10.5, and 8.5). The white and black regions correspond to the YAG and the Al_2O_3 phases, respectively. Within the composition range Al_2O_3–x mol%Y_2O_3 (x = 18.5, 15.0, and 13.5), the Al_2O_3 phase segregation was hardly observed, and the volume fraction of the Al_2O_3 phase increased from 37% (23.5 mol%Y_2O_3) to 64% (13.5 mol%Y_2O_3). In the composition of Al_2O_3–18.5 mol%Y_2O_3, which is the same composition as the unidirectional solidified Al_2O_3–YAG, the average value of lamellar spacing of the specimen was 2.7 μm, which was about 5 times smaller than that of unidirectional solidified Al_2O_3–YAG (14 μm).[3–5] Compared to the Al_2O_3–YAG eutectic fiber formed by using the micro-pulling down,[24,25] Edge-Defined-film-fed Growth (EFG) processing[24] and laser-heated float Zone method,[26] the lamellar spacing was of the same order as those of the Al_2O_3–YAG eutectic fiber. The relative density of Al_2O_3–YAG eutectic compacts with compositions of Al_2O_3–x mol%Y_2O_3 (x = 23.5, 18.5, 15.0, and 13.5) were 98%, 98%, 98%, and 96%, respectively. Al_2O_3–YAG eutectic compacts with high relative density (more than 96%) were formed by the addition of Al_2O_3 particles to Al_2O_3–YAP metastable eutectic particles.

On the other hand, in Al_2O_3–YAG eutectic compacts with compositions of Al_2O_3–x mol%Y_2O_3 (x = 10.5, and 8.5), Al_2O_3 phase segregation and many pores of diameter 2–5 μm in the vicinity of the Al_2O_3 grain boundaries were observed as shown in Fig. 3(e) and (f). The microstructure was essentially formed by sintering the added Al_2O_3 particles. The formation time of 60 s was too short to result in the formation of a dense compact.

3.2. Mechanical properties of Al_2O_3–YAG eutectic compact with off-metastable eutectic composition

The flexural strengths of Al_2O_3–YAG eutectic compacts with compositions of Al_2O_3–x mol%Y_2O_3 (x = 18.5, 15, and 13.5) produced by the addition of Al_2O_3 particles to Al_2O_3–YAP eutectic particles were measured. The average values of the flexural strength with compositions of Al_2O_3–x mol%Y_2O_3 (x = 18.5, 15, and 13.5) were 300, 370, and 330 MPa, respectively, compared with 339 MPa for the specimen of the Al_2O_3–23.5 mol%Y_2O_3. Although the flexural strength slightly increased for Al_2O_3–15 mol%Y_2O_3, the increase in the Al_2O_3 phase made almost no remarkable contribution to the improvement in room-temperature the flexural strength. Fig. 4 shows the variation of the flexural strength with the eutectic spacing for Al_2O_3–YAG eutectic compact with the composition of the Al_2O_3–18.5 mol%Y_2O_3 formed by using our method, unidirectional solidified Al_2O_3–YAG,[3–5]

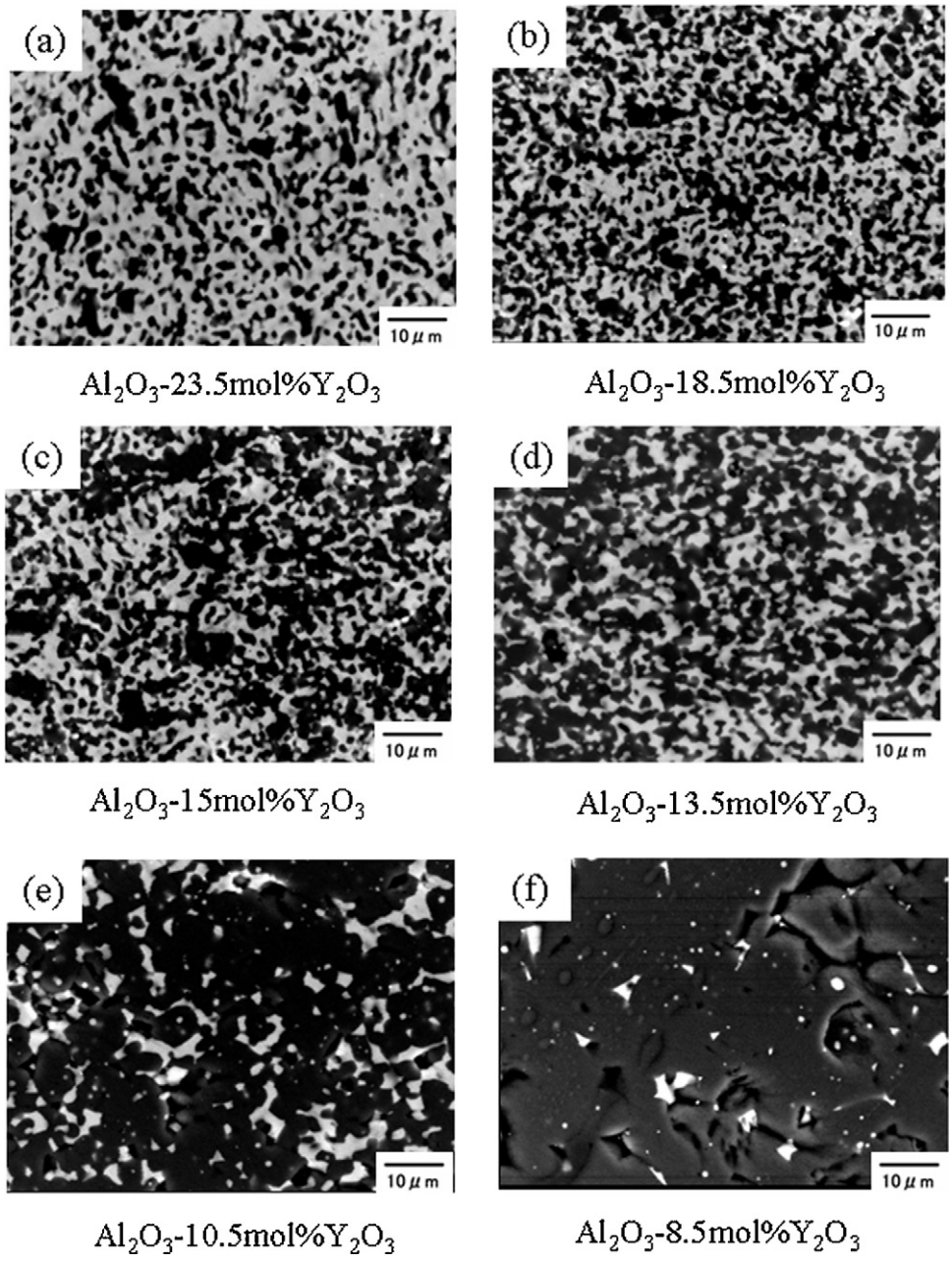

Fig. 3. Microstructures of Al_2O_3–YAG eutectic compacts with compositions of Al_2O_3–x mol%Y_2O_3: x = (a) 23.5 (b) 18.5 (c) 15.0 (d) 13.5 (e) 10.5, and (f) 8.5.

and Al_2O_3–YAG eutectic fiber.[27] The specimen with the composition of Al_2O_3–18.5 mol%Y_2O_3, which is the same composition as the unidirectional solidified Al_2O_3–YAG, showed almost the same room-temperature flexural strength as that of the unidirectional solidified Al_2O_3–YAG (350 MPa).[3–5] It has been reported that the flexural strength of the Al_2O_3–YAG eutectic is determined by the eutectic spacing.[24] The flexural strength depended on the lamellar spacing for the unidirectional solidified Al_2O_3–YAG and the Al_2O_3–YAG eutectic fiber. However, the Al_2O_3–YAG eutectic compact formed by using our method with a fine lamellar spacing, which was of the same order as the Al_2O_3–YAG eutectic fiber, showed no higher flexural strength than that of the unidirectional solidified Al_2O_3–YAG. The diameters of the Al_2O_3–YAG eutectic fiber generally ranges from 75 μm to 150 μm, whereas the dimension of the Al_2O_3–YAG eutectic compact produced by our method is several mm. The Al_2O_3–YAG compact can be more affected by the thermal expansion difference between the crucible and the eutectic material, which leads to the formation of the cracking.

The average values of the fracture toughness of Al_2O_3–YAG eutectic compacts with compositions of Al_2O_3–x mol%Y_2O_3 (x = 23.5, 18.5, 15, and 13.5) produced by the addition of Al_2O_3 particles to Al_2O_3–YAP eutectic particles are shown in Fig. 5. The fracture toughness of 2.7 MPa/m^2 for the Al_2O_3–YAG eutectic compact with the metastable eutectic composition (Al_2O_3–23.5 mol%Y_2O_3) almost remained unchanged over the

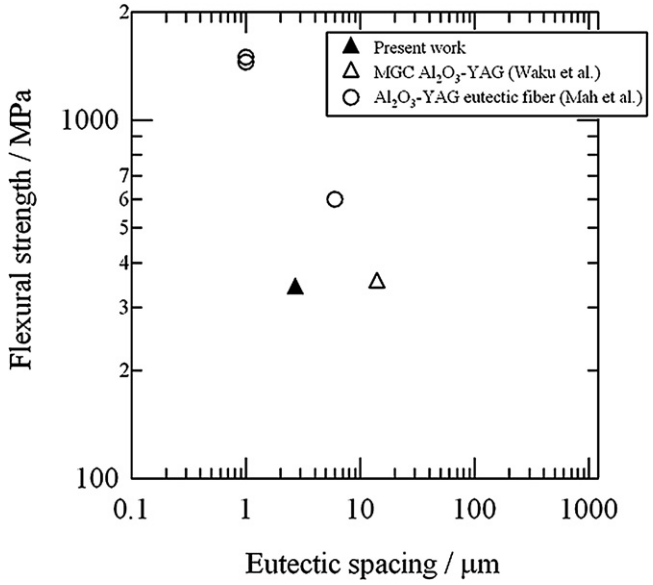

Fig. 4. The variation of flexural strength with eutectic spacing for (▲) Al_2O_3–YAG eutectic compact with the composition of the Al_2O_3–18.5 mol%Y_2O_3, (△) unidirectional solidified Al_2O_3–YAG (MGC Al_2O_3–YAG),[3–5] and (◯) Al_2O_3–YAG eutectic fiber.[27]

entire composition range. The fracture toughness of the unidirectional solidified Al_2O_3–YAG was 2–2.4 MPa $m^{1/2}$ [22] which was approximately equivalent to those of our specimens. Yang et al. reported that the Al_2O_3–YAG eutectic fiber grown by EFG process showed the fracture toughness of about 2 MPa/m^2.[28] This suggested that the fracture toughness in the Al_2O_3–YAG binary eutectic could not be explained simply by the lamellar spacing.

On the other hand, in compositions of Al_2O_3–x Y_2O_3 mol% (x = 10.5 and 8.5), it was impossible to carry out the three-point bending test and the Vickers hardness test because dense Al_2O_3–YAG eutectic compacts were not formed.

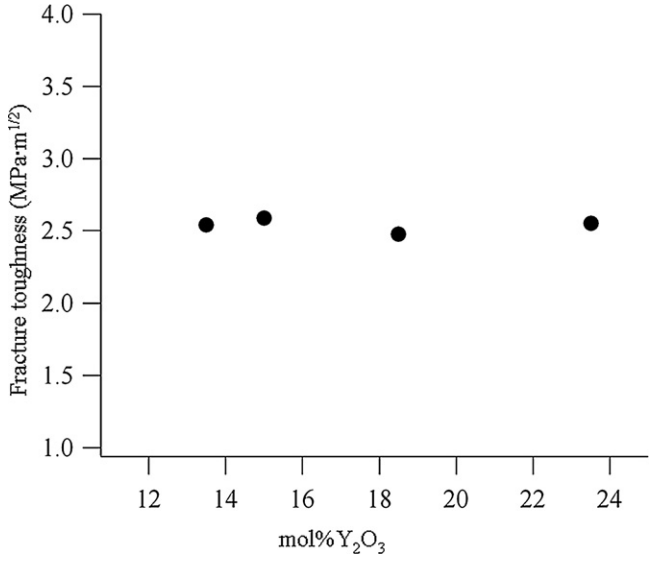

Fig. 5. Fracture toughness of Al_2O_3–YAG eutectic compacts as a function of mol%Y_2O_3.

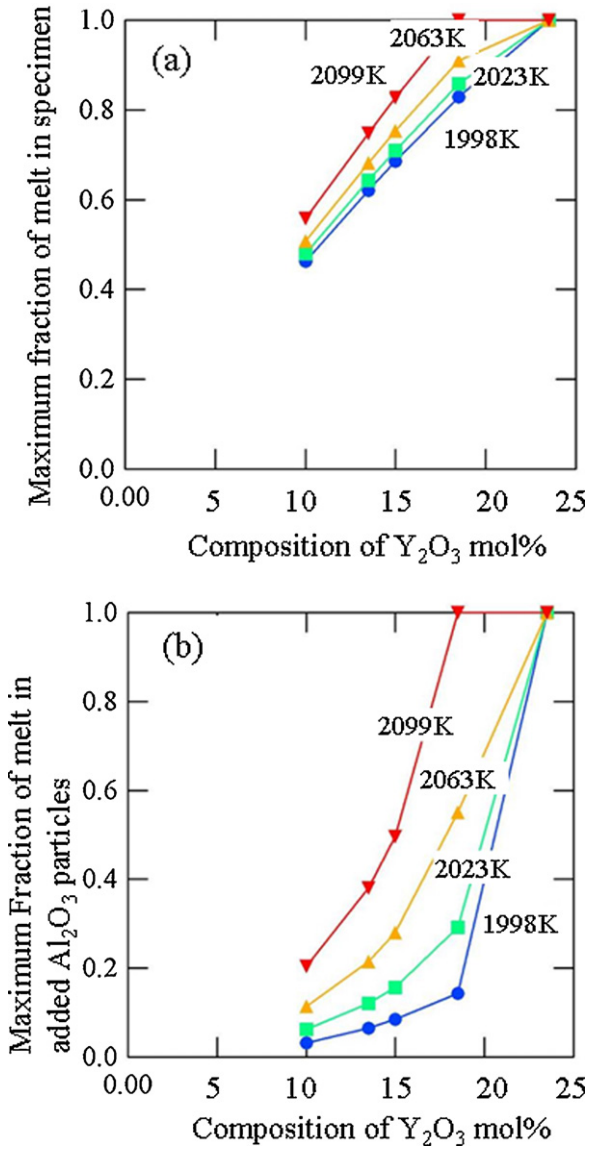

Fig. 6. Maximum fraction of melt in (a) specimen and (b) added Al_2O_3 particles as a function of Y_2O_3 mol% composition.

3.3. Influence of the addition of Al_2O_3 particles into the Al_2O_3–YAP eutectic particles on the formation of the Al_2O_3–YAG eutectic compact

The added Al_2O_3 particles were indistinguishable from that of the Al_2O_3–YAG eutectic structure produced by melting of Al_2O_3–YAP eutectic particles as shown in Fig. 3, suggesting that the added Al_2O_3 particles could be partially melted in the undercooled melt above the metastable eutectic temperature. Here, the melting of the added Al_2O_3 particles is considered in accordance with the phase equilibrium of the metastable eutectic system. The maximum melt fractions in the specimen and the added Al_2O_3 particles at 1998, 2023, 2063, and 2099 K as a function of the Al_2O_3–x Y_2O_3 mol% (x = 10, 13.5, 15.0, 18.5, and 23.5) were calculated using a lever principle, as shown in Fig. 6(a) and (b). Note that the Al_2O_3–YAP eutectic particles are completely melted to calculate the maximum fraction

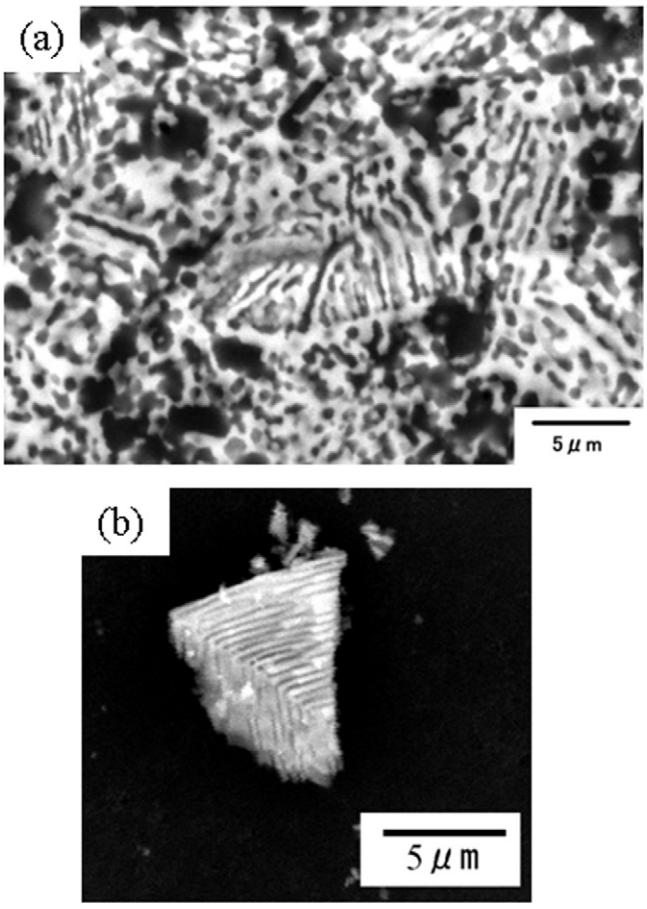

Fig. 7. Microstructures of (a) specimen with Al_2O_3–18.5 mol%Y_2O_3 heated at 1823 K and then rapidly cooled to room temperature, and (b) external appearance of Al_2O_3–YAP eutectic particles.

of melt in added Al_2O_3 particles. At the equilibrium eutectic temperature of 2099 K, a maximum of approximately 80% of the Al_2O_3–YAP specimen is melted for the composition of Al_2O_3–13.5 mol%Y_2O_3 and the maximum fraction of melt in added Al_2O_3 particles is calculated to be approximately 40%. On the other hand, although the maximum fraction of melt in the Al_2O_3–YAP specimen is approximately 60% at 2099 K for the Al_2O_3–10.0 mol%Y_2O_3, only 20% of the added Al_2O_3 particles are melted, even at the equilibrium eutectic temperature. Thus, in compositions with less than 10.0 mol%Y_2O_3, a large amount of the added Al_2O_3 particles remain unmelted in the undercooled melt. Because the microstructure is essentially formed by the sintering of the added Al_2O_3 particles, an Al_2O_3–YAG compact with many pores is formed due to the short sintering time of 60 s. This results correspond to the finding that the relative density decreases with an increase in the amount of added Al_2O_3.

The specimen with the composition of Al_2O_3–18.5 mol%Y_2O_3 was heated to 1923 K, which is 50 K lower than the metastable eutectic temperature, and then rapidly cooled to room temperature to observe the microstructure immediately before the melting of the specimen. Fig. 7(a) shows the microstructure consisting of unmelted Al_2O_3–YAP eutectic particles with a lamellar structure and spherical Al_2O_3 particles with a diameter of approximately 1 μm. For comparison, the external appearance of the Al_2O_3–YAP eutectic grains with a lamellar spacing of less than 1 μm is shown in Fig. 7(b). As shown in Fig. 7, Al_2O_3–YAP eutectic particles were sintered with the added Al_2O_3 particles; consequently, Al_2O_3/YAP phase boundaries were formed between the Al_2O_3–YAP eutectic particles and the added Al_2O_3 particles. Thus, the added Al_2O_3 particles melted at the Al_2O_3/YAP phase boundaries as well as the Al_2O_3–YAP eutectic particles. The addition of Al_2O_3 particles to Al_2O_3–YAP eutectic particles had a limitation in controlling the composition due to the increase in the fraction of unmelted Al_2O_3 particles as shown in Fig. 6(b), however, it is possible to form the dense Al_2O_3–YAG eutectic compacts without any Al_2O_3 segregation over the composition ranges of Al_2O_3–$x$$Y_2O_3$ mol% (x = 13.5, 15.0, and 18.5).

4. Conclusions

An Al_2O_3–YAG eutectic compact with an off-metastable eutectic composition was fabricated through the addition of Al_2O_3 particles with diameter of 1 μm to Al_2O_3–YAP eutectic particles with diameters of less than 20 μm. In compositions ranging from Al_2O_3–18.5 mol%Y_2O_3 to Al_2O_3–13.5 mol%Y_2O_3, the relative density was more than 96% and the Al_2O_3 phase was distributed almost homogeneously throughout the specimen. In the Al_2O_3–YAG eutectic compacts with compositions of Al_2O_3–x mol%Y_2O_3 (x = 10.5 and 8.5), the Al_2O_3 phase segregation and many pores with diameters of 2–5 μm were observed in the vicinity of the Al_2O_3 grain boundaries. The matrix phase shifted from the YAG phase (Al_2O_3–23.5 mol%Y_2O_3) to the Al_2O_3 phase (Al_2O_3–13.5 mol%Y_2O_3) as the amount of added Al_2O_3 increased. The increase in the Al_2O_3 phase hardly contributed to the improvement of the flexural strength (300–370 MPa) and the fracture toughness (2.5–2.7 MPa/m^2) at room temperature. Based on the phase equilibrium of the metastable eutectic system, the fraction of melting in the Al_2O_3–YAP specimen is approximately 80% for the composition of Al_2O_3–13.5 mol%Y_2O_3 at the equilibrium eutectic temperature whereas approximately 40% of added Al_2O_3 particles melted. The Al_2O_3–YAP eutectic particles and the added Al_2O_3 particles were consolidated at temperatures below the metastable eutectic temperature, suggesting that the undercooled melt is formed at the Al_2O_3/YAP phase boundaries between the added Al_2O_3 particles and Al_2O_3–YAP eutectic particles. The addition of Al_2O_3 particles to the Al_2O_3–YAP eutectic particles enables the formation of dense Al_2O_3–YAG eutectic compacts without any Al_2O_3 segregation in compositions ranging from Al_2O_3–13.5 Y_2O_3 mol% to Al_2O_3–18.5 Y_2O_3 mol%.

Acknowledgements

This work was supported by a Grant-in-Aid for Young Scientists (A) (No. 22686070) and a Grant-in-Aid for Scientific Research (A) (No. 20246112) from JSPS. This work was also partially supported by the MEXT Global COE Program (Project:

Center of Excellence for Advanced Structural and Functional Materials Design).

References

1. Mah T, Parthasarathy TA. Processing and mechanical properties of $Al_2O_3/Y_3Al_5O_{12}$ (YAG) eutectic composite. *Ceram Eng Sci Proc* 1990;**11**:1617–27.
2. Parthasarathy TA, Mah T. Creep behavior of an Al_2O_3–$Y_3Al_5O_{12}$ eutectic composite. *Ceram Eng Sci Proc* 1990;**9–10**:1628–38.
3. Waku Y, Nakagawa N, Wakamoto T, Ohtsubo H, Shimizu K. A ductile ceramics eutectic composite with high strength at 1873 K. *Nature* 1997;**389**:49–52.
4. Waku Y, Nakagawa N, Wakamoto T, Ohtsubo H, Shimizu K, Kohtoku Y. High-temperature strength and thermal stability of a unidirectionally solidified Al_2O_3/YAG eutectic composite. *J Mater Sci* 1998;**33**:1217–25.
5. Waku Y, Nakagawa N, Wakamoto T, Ohtsubo H, Shimizu K, Kohtoku Y. The creep and thermal stability characteristics of a unidirectionally solidified Al_2O_3/YAG eutectic composite. *J Mater Sci* 1998;**33**:4943–51.
6. Parthasarathy TA, Mah T. Deformation behavior of an Al_2O_3–$Y_3Al_5O_{12}$ eutectic composite in comparison with sapphire and YAG. *J Am Ceram Soc* 1993;**76**:29–32.
7. Randall SH. Kinetics and deformation during the reaction of yttrium–aluminum perovskite and alumina to yttrium–aluminum garnet. *J Am Ceram Soc* 1994;**77**:1473–85.
8. Caslavsky JL, Viechinickl DJ. Melting behaviour and metastability of yttrium aluminium garnet (YAG) and $YAlO_3$ determined by optical differential thermal analysis. *J Mater Sci* 1980;**15**:1709–18.
9. Yasuda H, Ohnaka I, Mizutani Y, Waku Y. Selection of eutectic systems in Al_2O_3–Y_2O_3 ceramics. *Sci Tech Adv Mater* 2001;**2**:67–71.
10. Yasuda H, Mizutani T, Ohnaka I, Sugiyama A, Waku Y. Production of undercooled melt by heating the metastable Al_2O_3–YAP eutectic structure. *Mater Trans* 2001;**42**:2124–30.
11. Mizutani Y, Yasuda H, Ohnaka I, Sugiyama A, Takeshima S, Kirihara M, et al. Undercooled melt formation by melting of metastable eutectic structure in Al_2O_3–Y_2O_3–ZrO_2 system. *Mater Trans* 2002;**43**:2847–54.
12. Mizutani Y, Yasuda H, Maeda N, Waku Y. Coupled growth of unidirectionally solidified Al_2O_3–YAG eutectic ceramics. *J Cryst Growth* 2002;**244**:384–92.
13. Yasuda H, Mizutani Y, Ohnaka I, Sugiyama A, Morikawa T. Undercooled melt formation and shaping of alumina–yttrium garnet eutectic ceramics. *J Am Ceram Soc* 2003;**86**:1818–20.
14. Yasuda H, Ohnaka I, Mizutani Y, Sugiyama A, Morikawa T, Takeshima S, et al. Solidification and shape casting of Al_2O_3–YAG eutectics from the undercooled melt produced by melting Al_2O_3–YAP eutectics. *Sci Tech Adv Mater* 2004;**5**:207–17.
15. Yasuda H, Ohnaka I, Sugiyama A, Mizutani Y, Sakimura T, Kawaguchi A, et al. Undercooled melt shaping of Al_2O_3–YAG eutectic composite by melting the Al_2O_3–YAP eutectic structure. *Mater Sci Form* 2005;**475–479**:2709–12.
16. Nagira T, Yasuda H, Sakimura T, Kawaguchi A. Effects of shaping conditions on the microstructure and the mechanical property of the Al_2O_3–YAG eutectic composite produced by melting the Al_2O_3–YAP eutectic structure. *Mater Trans* 2007;**48**:2312–5.
17. Nagira T, Yasuda H, Yoshiya M. Formation and microstructure of Al_2O_3–YAG eutectic ceramics by phase transformation from metastable system to equilibrium system. *J Phys Conf Ser* 2009;**165**:012006.
18. Hirano K. Application of eutectic composites to gas turbine system and fundamental fracture properties up to 1700 °C. *J Eur Ceram Soc* 2005;**25**:1191–9.
19. Harada Y, Uekawa N, Kojima T, Kakegawa K. Formation of $Y_3Al_5O_{12}$–Al_2O_3 eutectic microstructure with off-eutectic composition. *J Eur Ceram Soc* 2008;**28**:1973–8.
20. Su H, Zhang J, Song K, Liu L, Fu H. Investigation of the solidification behavior of Al_2O_3/YAG/YSZ ceramic in situ composite with off-eutectic composition. *J Eur Ceram Soc* 2011;**31**:1233–9.
21. Anstis GR, Chantikul P, Lawn BR, Marshall DB. A critical evaluation of indentation techniques for measuring fracture toughness. *J Am Ceram* 1981;**64**:533–8.
22. Larrea A, Orera VM, Merino RI, Pena JI. Microstructure and mechanical properties of Al_2O_3–YSZ and Al_2O_3–YAG directionally solidified eutectic plates. *J Eur Ceram Soc* 2005;**25**:1419–29.
23. Ochiai S, Sakai Y, Sato K. Fracture characteristics of Al_2O_3/YAG composite at room temperature to 2073 K. *J Eur Ceram Soc* 2005;**25**:1241–9.
24. Parthasarathy TA, Mah T, Matson LE. Processing, structure and properties of alumina–YAG eutectic composites. *J Ceram Proc Res* 2004;**5**:380–90.
25. Epelbaum BM, Yoshikawa A, Shimamura K, Fukuda T, Suzuki K, Waku Y. Microstructure of $Al_2O_3/Y_3Al_5O_{12}$ eutectic fibers grown by μ-PD method. *J Cryst Growth* 1999;**198/199**:471–5.
26. Frazer CS, Dickey EC, Sayir A. Crystallographic texture and orientation variants in Al_2O_3–$Y_3Al_5O_{12}$ directionally solidified eutectic crystals. *J Cryst Growth* 2001;**233**:187–95.
27. Mah T, Parthasarathy Petry D, Matson LE. Processing microstructure and properties of Al_2O_3–$Y_3Al_5O_{12}$(YAG) eutectic fibers. *Ceram Eng Sci Proc* 1993;**14**:622–38.
28. Yang JM, Jeng SM, Chang S. Fracture behavior of directionally solidified $Y_3Al_5O_{12}/Al_2O_3$ eutectic fiber. *J Am Ceram Soc* 1996;**79**:1218–22.